

A Computational Efficient Algorithm for the Design of a Line Start Synchronous Motor with Multi-Segment Magnet Rotor

Yannis L. Karnavas, *Member, IEEE*, and Ioannis D. Chasiotis, *S. Member, IEEE*

Abstract—Line start permanent magnet synchronous motors present many advantages therefore are considered as an attractive choice for being induction motors alternatives. In this context, this paper presents an analytical though simple algorithmic approach for determining the geometrical characteristics of a multi-segment magnet rotor as a replacement of an already designed and optimized induction motor counterpart. Three different rotor geometries and eight magnet alloys are examined through simulations to validate the proposed algorithm's efficiency. Moreover the manufacturing cost is calculated while the target is to minimize the magnet weight. The relevant results showed that the proposed algorithm performs satisfactorily as an aid design tool. The feasibility of the replacement of the induction motor's rotor with a multi-segment magnet synchronous motor rotor was also confirmed in terms of economic and operational viability.

Index Terms—Line start permanent magnet synchronous motor, multi-segment magnet rotor, electrical machines design.

I. INTRODUCTION

PERMANENT magnet synchronous motors (PMSM) with buried magnets have been considered in a wide range of either fixed or variable speed drives. Also, a buried magnet design has many advantages compared to designs with surface mounted and inset magnets. With a buried magnet design, flux concentration can be achieved, which induces higher air gap flux density. That, in turn, gives a possibility to increase the torque of the machine. The buried magnet construction also gives a possibility to create a non-uniform air gap resulting smoother torque and more sinusoidal currents [1], [2]. Arranging the permanent magnets (PM) in a V-magnet shape is a good solution for this kind of applications as it produces a high reluctance torque next to the PM torque. This leads to an advantage in efficiency as the field weakening current needed above rated speed is also torque-producing. Additionally, it

decreases the dependency of the design on temperature variations according to the temperature dependency of the PM flux. Of course, since the used rare-earth magnets have a great effect on the machine costs it is advantageous to reduce the needed magnet volume per torque. This is a motivation to produce a high share of torque through the reluctance effect [3], [4]. The use of multi-layer magnets has also been proposed as it gives saliency to the machine thus increasing the reluctance torque even more. This effect, results to higher output torque in a wider speed range, comparing to the single-layer topology. However, the increase in the magnets number is accompanying by a larger cost, while the mechanical strength and durability are reduced as the number of layers are getting larger [5].

On the other hand, high efficiency induction motors (IM) obtain higher efficiency than standard IMs but with a lower power factor at the same time. Moreover, they are quite material-consuming. The simplest way to increase an IM's efficiency, its power factor, its simplicity, its mechanical robustness and its inherent self-starting property, is the replacement of the standard squirrel-cage rotor with a squirrel-cage permanent magnet rotor and, consequently, change the IM into a line start permanent magnet synchronous motor (LS-PMSM) [6]-[8]. This can be fulfilled by the proper selection of a) the rotor's inner (shaft) and outer diameter, and b) the widths and displacements of the magnet segments. Although finite element analysis (FEA) is an accurate method for this purpose, it is very time consuming in finding optimal configuration due to the exponentially large number of simulations needed. Thus, an algorithmic based design optimization may be very useful and eases the design process [9].

In this paper, a simple algorithm for the calculation of the rotor topology characteristics in candidate LS-PMSMs is proposed. Based on an already designed IM stator, a multi-variable determination framework is developed. It was found that the algorithm needs a small number of iterations until convergence to an optimal machine design solution. Three rotor types were examined, each one by eight commercially available magnet types. Materials consumptions were also taken into account, while the desired motor torque, power factor and efficiency achieved.

Y. L. Karnavas is with the Department of Electrical and Computer Engineering, Democritus University of Thrace, Xanthi, Hellas (GR), (e-mail: karnavas@ee.duth.gr).

I. D. Chasiotis is with the Department of Electrical and Computer Engineering, Democritus University of Thrace, Xanthi, Hellas (GR), (e-mail: ioanchas@ee.duth.gr).

II. INDUCTION MOTOR MODEL UNDER CONSIDERATION

A three-phase squirrel-cage induction motor (SCIM) is considered here with nominal values and specification data as per the Appendix (Table XI). Since the emphasis here is on the LS-PMSM rotor design, the SCIM's design is just presented here (also in the Appendix, Table XII), so the reader can verify and check the validity of our further results obtained. It should be stated though, that these data refer to an actual commercial motor and derived through FEA calculations based on its name plate's data only. With respect to Table XII, Fig. 1 depicts the used SCIM's rotor and stator geometries along with the relevant variables (diameters, widths and bores). The reader can refer i.e. to [10]-[12] for further analysis in SCIM performance through finite elements technique.

III. SINGLE AND MULTI-SEGMENT MAGNET TOPOLOGIES

As aforementioned, in interior PM motors, permanent magnets are embedded in the rotor, so that a reluctance torque is generated in addition to the magnet torque. Furthermore, the induced voltage can be reduced by canceling the magnetic flux of the permanent magnets by field-weakening control; this and other features contribute to a wider range of high-speed operation, and such motors are used for various applications. Two common single-segment magnet rotor constructions of interior type are the tangential and the radial topology [13].

The magnetic field system of interior PM motors is based on rare-earth sintered magnets, and the magnets are usually designed as rectangles considering manufacturing cost. In addition, the magnets are often arranged in one or more layers to enhance the reluctance torque as well as for other purposes [14]-[15]. In this case, various arrangements of rectangular magnets may be considered. However, very few studies compare the advantages and disadvantages of different options i.e. in [17], [18].

Continuing, magnet segmentation is an effective and simple technique especially for cogging torque reduction in high power PMSMs; however, if the segmentation is not optimal the air gap flux density is deteriorated and the output torque is decreased. In a segmented PM machine, each pole is divided into several elementary blocks positioned beside each other whereas there is a specific opening between adjacent blocks. These openings can be filled with some nonmagnetic material to reduce air turbulence effect at high rotational speeds. In this work, we consider these gaps (also called "bridges") filled with air since the required speed is medium. Moreover, PM pieces may have equal or unequal widths. Once the total width is determined, the share of each block can be calculated through simple geometrical formulas. Finally, magnet types and magnetization direction of all blocks are considered the same. Fig. 2 shows the schematic views of the three 4-pole, multi-segment magnet rotors used in this study namely: V-

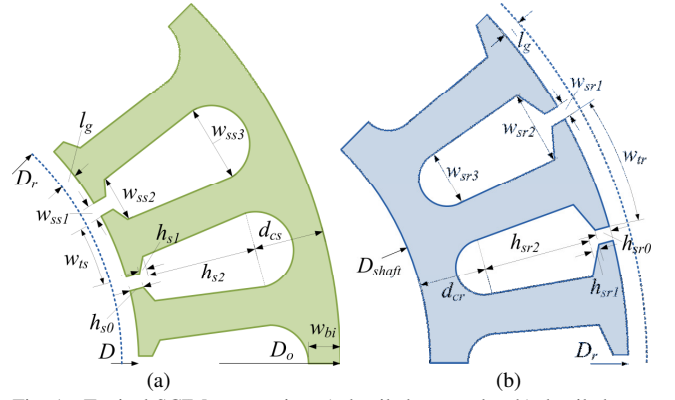


Fig. 1. Typical SCIM geometries: a) detailed stator slot, b) detailed rotor slot. The latter is being replaced here by a multi-segment magnet rotor.

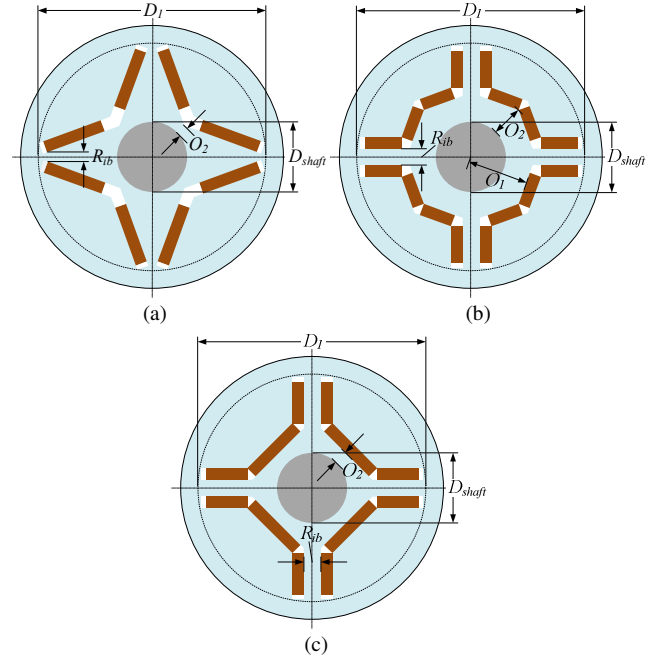


Fig. 2. Multi-segment magnet rotor configurations under investigation, (a) V-shape, b) double V-shape, c) U-shape.

shape, double-V shape and U-shape. We denote these rotors by "A", "B" and "C" respectively for our further reference. There are many ways that each one of these geometries can be expressed. Here, the sufficient variables involved are: a) the shaft diameter (D_{shaft}), b) the inner diameter (D_l) which actually gives the depth from the rotor surface at which the magnets start, c) the closest distance between two adjacent pole magnets (R_{ib}), d) the closest distance between the outer circumference of the motor shaft and the middle point (vertical axis of symmetry) of the whole magnet pole (O_2), e) the vertical distance from the centre of the machine to the side of a middle magnet segment (O_1 in "B" type rotor only) and f) the magnet segments total width (w_m) and height (h_m).

IV. PROPOSED ALGORITHM AND RESULTS

With respect to Fig. 2, each topology may be described by different number N of variables (i.e. D_l , O_2 , O_1 , R_{ib} etc.).

Let us denote as V_i ($i=1..N$) the values of these variables. Then, the main steps of the algorithm can be described as:

Step 1: Each variable is initiated to a random value inside its universe of discourse and an appropriate step is defined for it.

Step 2: For every variable, an iteration loop is initiated. If every variable has been examined the algorithm stops.

Step 3: Iteration advances. The run-time engine of a commercial FEA software is called, magnetic field analysis is performed and quantities of concern (i.e. torque, power factor, efficiency, cost) are calculated.

Step 4: If the performance quantities' values are better than the previous ones, the variable value where that happened is fixed for future use and the procedure continues with Step 5, else with Step 3.

Step 5: Especially for the magnets' variables, the values which are stored refer to those giving the least cost.

Step 6: Variable index increases and the procedure continues with Step 2, else the algorithm stops.

The corresponding flowchart is depicted in Fig. 3. The algorithm was written in a programming script language and was integrated to a well known commercial finite element analysis software. Continuously, it was applied to the three aforementioned rotor topologies and the procedure also

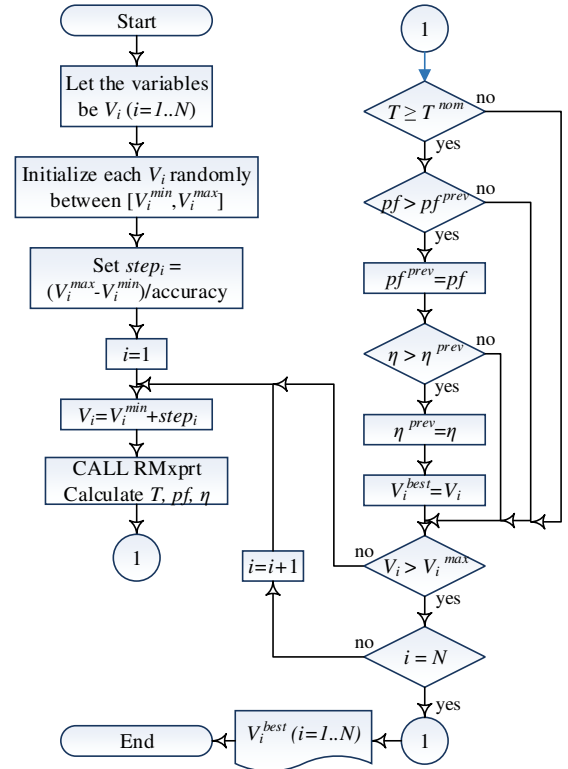


Fig. 3. Flowchart of the proposed algorithm.

TABLE I
CALCULATED VALUES OF ROTOR "A" GEOMETRY (IN MM).

Magnet Type	D_1	O_2	R_{ib}	D_{shaft}	w_m	h_m
Alnico5	70.4	5.9	7.5	38	32.1	5.0
Alnico9	70.4	0.0	0.0	38	33.5	3.0
SmCo24	70.4	2.0	2.0	39	34.8	3.0
SmCo28	70.4	2.0	2.0	38	28.0	4.0
NdFe30	70.4	2.0	2.0	38	33.0	3.0
NdFe35	70.4	1.0	1.0	33	32.2	2.9
Ceramic5	70.4	2.0	2.0	34	35.7	7.0
Ceramic8D	70.4	2.0	2.0	34	35.0	7.0

TABLE II
CALCULATED VALUES OF ROTOR "B" GEOMETRY (IN MM).

Magnet Type	D_1	O_2	O_1	R_{ib}	D_{shaft}	w_m	h_m
Alnico5	70.4	12.0	27.0	19.0	38.0	30.0	3.0
Alnico9	70.4	12.0	27.0	9.0	38.0	31.0	3.0
SmCo24	70.4	12.0	27.0	9.0	38.0	33.0	3.0
SmCo28	70.4	12.0	27.0	9.0	38.0	31.0	3.0
NdFe30	70.4	12.0	27.0	9.0	38.0	30.0	3.0
NdFe35	70.4	12.0	27.0	9.0	38.0	30.0	3.0
Ceramic5	70.4	12.0	27.0	9.0	38.0	42.0	3.0
Ceramic8D	70.4	12.0	27.0	9.0	38.0	42.0	3.0

TABLE III
CALCULATED VALUES OF ROTOR "C" GEOMETRY (IN MM).

Magnet Type	D_1	O_2	R_{ib}	D_{shaft}	w_m	h_m
Alnico5	70.4	3.0	6.0	37.0	30.0	5.3
Alnico9	70.4	2.0	6.0	37.0	27.3	4.7
SmCo24	70.4	2.0	6.0	37.0	28.2	5.1
SmCo28	70.4	2.0	6.0	37.0	27.4	4.4
NdFe30	70.4	2.0	6.0	37.0	27.1	4.2
NdFe35	70.4	2.0	6.0	37.0	26.0	3.4
Ceramic5	70.4	2.0	6.0	37.0	33.3	8.0
Ceramic8D	70.4	2.0	6.0	37.0	33.3	8.0

TABLE IV
CALCULATED PERFORMANCE QUANTITIES OF LS-PMSM WITH ROTOR "A".

Magnet Type	T (Nm)	η (%)	pf
Alnico5	10.158	89.992	0.999
Alnico9	10.158	89.992	0.999
SmCo24	10.158	89.992	0.999
SmCo28	10.159	89.992	0.999
NdFe30	10.158	89.992	0.999
NdFe35	10.158	89.992	0.999
Ceramic5	10.161	88.909	0.955
Ceramic8D	10.165	88.933	0.957

TABLE V
CALCULATED PERFORMANCE QUANTITIES OF LS-PMSM WITH ROTOR "B".

Magnet Type	T (Nm)	η (%)	pf
Alnico5	10.159	89.854	0.994
Alnico9	10.158	89.992	0.999
SmCo24	10.158	89.992	0.999
SmCo28	10.158	89.992	0.999
NdFe30	10.158	89.992	1.000
NdFe35	10.158	89.992	0.999
Ceramic5	10.166	88.405	0.937
Ceramic8D	10.163	88.450	0.939

TABLE VI
CALCULATED PERFORMANCE QUANTITIES OF LS-PMSM WITH ROTOR "C".

Magnet Type	T (Nm)	η (%)	pf
Alnico5	10.158	89.992	0.999
Alnico9	10.159	89.992	0.999
SmCo24	10.159	89.992	0.999
SmCo28	10.159	89.992	0.999
NdFe30	10.159	89.992	0.999
NdFe35	10.158	89.992	0.999
Ceramic5	10.172	88.871	0.955
Ceramic8D	10.170	88.901	0.956

TABLE VII
CALCULATED ROTOR MATERIAL CONSUMPTIONS AND COST OF ROTOR "A"
FOR DIFFERENT MAGNET TYPES.

Magnet type	Rotor Cage material consumption (gr)	Magnetic material consumption (gr)	Rotor Core material consumption (kgr)	Overall Rotor Cost (USD)
Alnico5	96.0	492.093	6.377	27.77
Alnico9	96.0	308.333	6.377	19.66
SmCo24	96.0	363.938	6.377	62.24
SmCo28	96.0	390.932	6.377	66.40
NdFe30	96.0	313.929	6.377	36.65
NdFe35	96.0	290.225	6.377	30.29
Ceramic5	96.0	514.294	6.377	8.33
Ceramic8D	96.0	504.210	6.377	8.29

TABLE VIII
CALCULATED ROTOR MATERIAL CONSUMPTIONS AND COST OF ROTOR "B"
FOR DIFFERENT MAGNET TYPES.

Magnet type	Rotor Cage material consumption (gr)	Magnetic material consumption (gr)	Rotor Core material consumption (kgr)	Overall Rotor Cost (USD)
Alnico5	96.0	279.720	6.377	18.40
Alnico9	96.0	285.138	6.377	18.64
SmCo24	96.0	345.114	6.377	59.33
SmCo28	96.0	313.740	6.377	54.49
NdFe30	96.0	266.364	6.377	26.62
NdFe35	96.0	233.100	6.377	24.05
Ceramic5	96.0	259.308	6.377	7.21
Ceramic8D	96.0	253.134	6.377	7.18

TABLE IX
CALCULATED ROTOR MATERIAL CONSUMPTIONS AND COST OF ROTOR "C"
FOR DIFFERENT MAGNET TYPES.

Magnet type	Rotor Cage material consumption (gr)	Magnetic material consumption (gr)	Rotor Core material consumption (kgr)	Overall Rotor Cost (USD)
Alnico5	96.0	496.692	6.377	27.90
Alnico9	96.0	393.398	6.377	23.41
SmCo24	96.0	501.357	6.377	83.45
SmCo28	96.0	420.272	6.377	70.93
NdFe30	96.0	360.923	6.377	33.92
NdFe35	96.0	274.747	6.377	27.27
Ceramic5	96.0	548.251	6.377	8.48
Ceramic8D	96.0	548.251	6.377	8.48

repeated for 8 different magnet materials (4 types by 2 grades), thus a total of 24 result sets obtained. Tables I-III show the corresponding geometrical (core and magnet) final values for each magnet type. It is reminded that, specifically for the magnet width w_m the calculated value refer to the total width of all the segments involved per pole. The software then "splits" this width by applying simple geometrical formulas regarding each segment. For example, in U-shape magnet, if l_1 is the length of the middle segment, l_2 is the length of the side segments ($l_1 + 2l_2 = w_m$), and b_w the total bridge width, then l_2 (with $R_{ib}=0$) can be expressed as:

$$l_2 = \frac{\sqrt{2}(D_1 - h_m - 2b_w) - (D_{shaft} + 2O_2 + h_m + w_m/2)}{2(\sqrt{2}-1)} \quad (1)$$

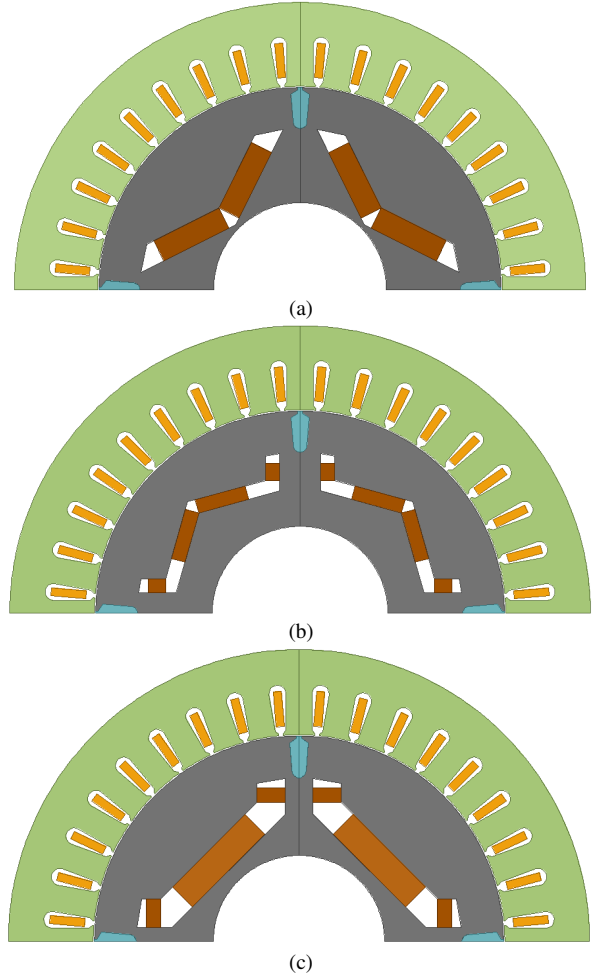


Fig. 4. Rendered cross sections of the final optimized multi-segment magnet rotors a) rotor "A", b) rotor "B" and c) rotor "C".

It can be observed from these Tables, that the variables which refer to the rotor core only are found quite constant for each magnet type, while the variables which refer to the magnet segments are clearly different, which is true in terms of magnet energy density. Also, by calculation of the area of the magnet segments, it is seen that for rotor "A", NdFe magnets require 2.5 times less area per pole ($\sim 93\text{-}99\text{mm}^2$) compared to e.g. ceramic ones ($\sim 250\text{mm}^2$). In rotor "B" though, it is seen that Alnico5 "scores" the same area with NdFe magnets ($\sim 90\text{mm}^2$) but with a different R_{ib} . Tables IV-VI show the calculated final performance quantities (torque, power factor and efficiency) for each case. As it is displayed, all magnet alloys reached the desired torque and also outperformed for efficiency ($\sim 90\%$) and power factor (~ 1.0). As expected, ceramic alloys were somewhat worse in term of the latter two quantities, but still better than IM specifications.

The materials consumptions (core, cage and magnets) for the resulted rotors were calculated along with their corresponding cost through international markets (i.e. www.infomine.com) and are shown in Tables VII-IX. Considering the fact that the original IM's rotor total cost

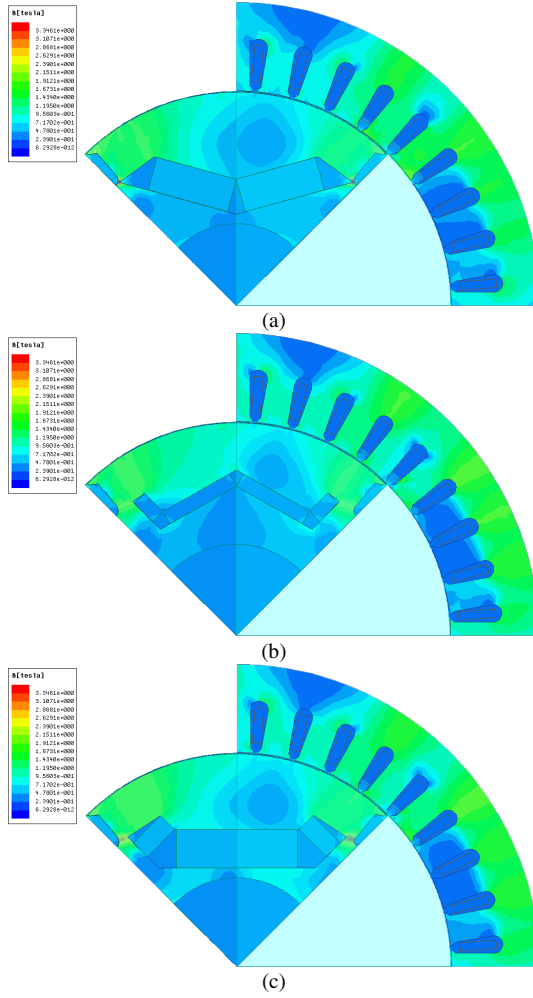


Fig. 5. Magnetic flux density distribution plot of the final optimized and designed multi-segment magnet rotors (in motor running mode), a) rotor "A", b) rotor "B" and c) rotor "C". Scale is the same for all of them.

was found \$7.11 (not shown here), the most competitive alloys it is clearly the ceramic ones for all rotor types, which exhibits similar cost. On the other hand, if NdFe alloy is chosen to be used, rotor "B" (double-V shape) rotor type is the most preferable which comes approximately 3.5 times more expensive. Finally, w.r.t. Tables I-III, the cross sections of the final configurations of the LS-PMSM, comprising of the IM's stator and the three multi-segment magnet rotor types examined are depicted in Fig. 4. The relevant flux density distribution plots (in motor running condition) are shown in Fig. 5, where the air-gap flux density lies in the 1.1-1.3T region which is considered quite satisfactory. The above performance analysis and comparisons have been conducted by setting 20°C as permanent magnets' working temperature. However, some of the PMs used (Alnico and Ceramic) are low energy alloys and are under risk to be demagnetized. In that context, demagnetization analysis was performed also for these materials, considering one medium and one high temperature (as the worst operating temperature, which may arise i.e. under fault conditions). Table X, shows the torque percentage loss (comparing to the nominal torque) due

TABLE X
CALCULATED LSPMSM'S TORQUE PERCENTAGE LOSS DUE TO PERMANENT MAGNET DEMAGNETIZATION EFFECT.

	Temp. (°C)	Rotor Type "A"	Rotor Type "B"	Rotor Type "C"
Ceramic8D	80	-18.91%	-28.22%	-20.21%
	140	-48.84%	-62.04%	-53.02%
Alnico9	80	-20.71%	-30.85%	-30.67%
	140	-26.87%	-33.40%	-46.87%

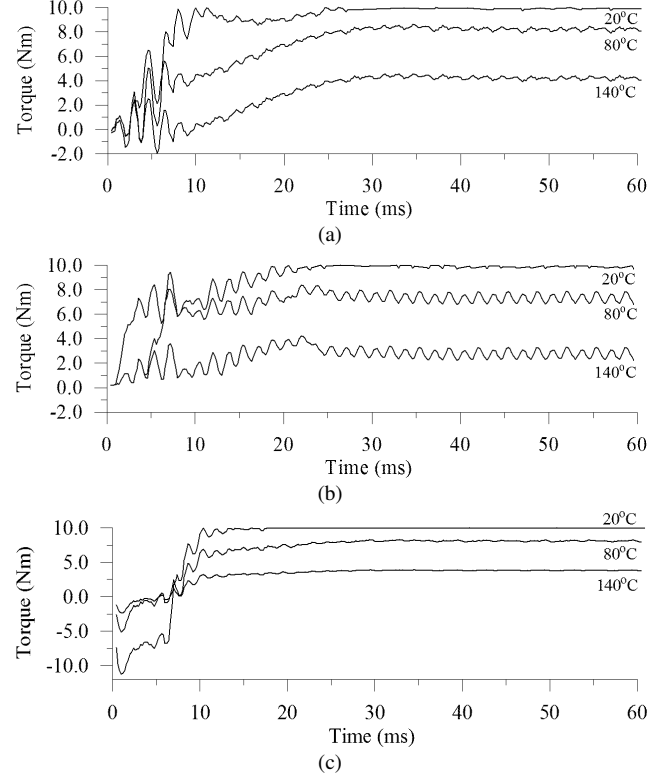


Fig. 6. LSPMSM torque related to the magnet (Ceramic8D) working temperature (20°C, 80°C, 140°C) for rotors, a) "A", b) "B" and c) "C".

to demagnetization for these working conditions, while Fig. 6 depicts the relevant time responses for each rotor type and Ceramic8D alloy. It can be easily seen that these two alloys fail to perform satisfactorily, while the rest (NdFe and SmCo) succeed (not shown here) due to their B-H curves.

V. CONCLUSIONS

A simple but effective algorithm presented in the paper as a quick aid tool for the design of multi-segment magnet rotors of line-start PMSMs. The algorithm applied by means of simulation to three different type of rotors for eight different magnet types and as a demonstration task was selected the rotor replacement of a real induction motor. The main advantage found to be the low number of iterations needed, thus minimizing the required computational time. The designed rotors contributed to the final motor successfully in terms of desired torque, power

factor and efficiency. Moreover, the relative material consumptions were calculated and in certain cases the overall rotor's cost found competitive to the original one. Further work may include the enhancement of the algorithm to be applied to multi-layer multi-segment magnet rotors, its influence on the reduction of the cogging torque and comparative assessments with other search techniques such as genetic algorithm, pattern search method and particle swarm optimization.

VI. APPENDIX

TABLE XI

THREE-PHASE SCIM SPECIFICATIONS (DESIRED) DATA.

Quantity	Symbol	Value	Unit
Output power	P_{out}	1500	[W]
Output Torque	T_{out}	10.15	[Nm]
Nominal speed	n	1410	[rpm]
Synchronous speed	n_s	1500	[rpm]
Nominal Voltage	V_n	380	[V]
Nominal frequency	f_n	50	[Hz]
Nominal slip	s	6%	-
Efficiency	η	75%-80%	-
Power factor	pf	> 0.78	-

TABLE XII

OPTIMAL CALCULATED GEOMETRICAL PARAMETERS OF THE THREE-PHASE SCIM UNDER STUDY (ALL DIMENSIONS IN [MM]).

Quantity	Stator	Value	Rotor	Value
Slot width at teeth	w_{ss1}	1.000	w_{sr1}	0.429
Slot width at opening	w_{ss2}	2.252	w_{sr2}	2.480
Slot width at end	w_{ss3}	3.650	w_{sr3}	5.200
Teeth width	w_{ts}	5.690	w_{tr}	6.134
Slot height at teeth	h_{s0}	0.333	h_{sr0}	0.600
Slot height at opening	h_{s1}	0.666	h_{sr1}	0.600
Slot height at end	h_{s2}	8.050	h_{sr2}	7.600
Iron bore width	w_{bi}	7.414	l_g	0.290
Core depth	d_{cs}	9.239	d_{cr}	9.239
Airgap diameter	D	89.000	D_{shaft}	46.636
Outer diameter	D_o	125.668	D_r	88.420

VII. REFERENCES

- [1] S. Hahlbeck, D. Gerling, "Design considerations for rotors with embedded V-shape permanent magnets", in *Proc. of the 18th Intl. Conference on Electrical Machines*, (ICEM), 2-5 Sep. 2008, Vilamora, Portugal, cd Ref. no. 908.
- [2] Y. Katsumi, K. Kazuya, "Optimization of magnet arrangement in double-layer interior permanent-magnet motors", *Electrical Engineering in Japan*, vol. 183, no. 4, 2013, pp. 54-62.
- [3] K. C. Kim, J. Lee, H. J. Kim, D. H. Koo, "Demagnetization analysis of permanent magnets according to rotor types of interior permanent magnet synchronous motor", *IEEE Transactions on Magnetics*, vol. 45, no. 6, 2009, pp. 2799-2802.
- [4] S.H. Han, T. M. Jahns, Z. Q. Zhu, "Analysis of rotor core eddy-current losses in interior permanent magnet synchronous machines", *IEEE Trans. in Industry Appl.*, vol. 46, no. 1, 2009, pp. 196-205.
- [5] S. Y. Kwak, J. K. Kim, H. K. Jung, "Characteristic analysis of multilayer-buried magnet synchronous motor using fixed permeability method", *IEEE Transactions on Energy Conversion*, vol. 20, no. 3, 2005, pp.549-555.
- [6] J. Parrish, S. Moll, R. C. Schaefer, "Synchronous versus induction motors: plant efficiency benefits resulting from the use of synchronous motors", *IEEE Industry Magazine*, vol. 12, no. 2, Mar.-Apr. 2006, pp. 61-70.

- [7] S.T Boroujeni, N. Bianchi, L. Alberti, "Fast estimation of line-start reluctance machine parameters by finite element analysis", *IEEE Trans. on Energy Conversion*, vol. 26, no. 1, Mar. 2011, pp.1-8.
- [8] J. Soullard, H.P. Nee, "Study of the synchronization of line-start permanent magnet synchronous motors" in *Proc. IEEE Ind. Appl. Conf. Rec.* 2000, vol. 1, Oct. 2000, pp. 424-431.
- [9] M. Ashabani, Y. Abdel-Rady, I. Mohamed, "Multi-objective Shape Optimization of Segmented Pole Permanent-Magnet Synchronous Machines with Improved Torque Characteristics", *IEEE Transactions on Magnetics*, vol. 47, no. 4, 2011, pp.795-804.
- [10] L. Alberti, N. Bianchi, S. Bolognani, "Variable-speed induction machine performance computed using finite-element", *IEEE Transactions on Industry Applications*, vol. 47, no. 2, Mar./Apr. 2011, pp. 789-797.
- [11] D. Dolinar, R. de Weerd, R. Belmans, E.M. Freman, "Calculation of two-axis induction motor model parameters using finite elements", *IEEE Trans. Energy Conv.*, vol. 12, no. 2, Jun. 1997, pp. 133-142.
- [12] S. Williamson, J.W. Ralph, "Finite-element analysis of an induction motor fed from a constant-voltage source" *IEE Proc. B, - Electric Power Applications.*, vol. 130, no. 1, Jan. 1983, pp. 18-24.
- [13] J. Kolehmainen, J. Ikaheimo, "Motors with buried magnets for medium-speed applications", *IEEE Transactions on Energy Conversion*, vol. 23, no. 1, 2008, pp. 86-91.
- [14] M. Sanada, K. Hiramoto, S. Morimoto, Y. Takeda, "Torque ripple improvement for synchronous reluctance motor using an asymmetric flux barrier arrangement", *IEEE Transactions on Industry Applications*, vol. 40, no. 4, 2004, pp. 1076-1082.
- [15] IEEJ Technical Committee, "Reluctance torque motors and control systems", IEEJ Tech. Rep. No. 719, Feb. 1993.
- [16] J. Kolehmainen, "Finite element analysis of two PM-motors with buried magnets" presented at the ICEM, Cracow, Poland, 2004, (Springer, 2006, S. Wiak, M. Dems, and K. Komeza, Eds., *Recent Developments of Electrical Drives*, Nov. 2006 , pp. 51-58.
- [17] Y. F. Shi, Z. Q. Zhu, D. Howe, "Torque-speed characteristics of interior-magnet machines in brushless AC and DC modes, with particular reference to their flux-weakening performance", in *Proc. of 5th IEEE Intl. Power Electronics and Motion Control Conference (IPEMC)*, 14-16 Aug., 2006, Shanghai, China, pp. 1-5.
- [18] P. W. Huang, S. H. Mao, M. C. Tsai, C. T. Liu, "Investigation of line start permanent magnet synchronous motors with interior-magnet rotors and surface-magnet rotors", in *Proc. of Intl. Conference on Electrical Machines and Systems (ICEMS)*, 17-20 Oct., 2008, Wuhan, China, pp. 2888-2893.

VIII. BIOGRAPHIES

Yannis L. Karnavas (M'98) was born in Volos, Hellas, 1969. He received his Ph.D. from the Department of Electrical & Computer Engineering (DECE), Democritus University of Thrace (DUTH), Xanthi, Hellas in 2002. He is with the Electrical Machines Laboratory of the DECE, DUTH as an Assistant Professor. His research interests include electrical machines design, analysis and modeling, controller design and application to electrical machines and artificial intelligence methods application to them. He has published several papers in various international journals and conferences as well as book chapters in international engineering books. He has participated in many research projects as research leader or scientific associate. He serves as an Associate Editor and as an Editorial board member in various international scientific journals. He is a chartered electrical engineer as well as a member of Hellenic Technical Chamber. Prof. Karnavas is also an IEEE PES, IAS and IES member.

Ioannis D. Chasiotis (St.M'11) was born in Athens, Hellas, 1991. He is a graduate of the Department of Electrical and Computer Engineering, Democritus University of Thrace, Xanthi, Hellas. He is with the Electrical Machines Laboratory of the same Department where he is currently pursuing his Ph.D. degree. His research interests are in the electrical machines design area and the development of relevant optimization methods and applications.